The Design of a Look-Down Feedback Adaptive Controller for the Lateral Control of Front-Wheel-Steering Autonomous Highway Vehicles

Seibum B. Choi

***Abstract*—An adaptive control law and a distance rate observer were developed for the lateral control of autonomous vehicles. The control law and the observer were implemented on a passenger vehicle. The test results show that both tight lateral tracking control and smooth steering can be achieved without feed forward information. The developed control law is shown to be very robust to changes in the most critical vehicle control parameters.**

***Index Terms*—Adaptive, autonomous, control, vehicle.**

I. Introduction

THERE HAVE been several studies to develop automated highways where automated vehicles are driving down the road, either individually or in platoons of multiple vehicles. Intelligent vehicle highway system (IVHS) aims to achieve congestion-free and accident-free highways by maximizing the capacity of highways and minimizing the driver-oriented accidents which are known to be the main source of car accidents [13].

The automated steering control of vehicles has been studied as part of IVHS [1], [2], [4], [5], [7], [13]. The lateral sensing is classified into look-ahead and look-down sensing. Look-ahead sensing can be realized using vision sensors [4], [11], [12]. Look-down sensing is classified into continuous and discontinuous sensing. It can be realized using electrified wires [2], radar reflection [8], or buried permanent magnets [6], [7]. Each sensing scheme has advantages and disadvantages. The vision sensor has the advantage of look-ahead, which makes the closed-loop control system more stable. However, it is expensive to acquire and to process the optical images into credible data in real-time in any weather and road conditions. The look-down sensing schemes using either electrified wires or permanent magnets can be realized by inexpensive sensors and simple data processing, and are guaranteed to work well in any weather and road conditions, but these schemes give no idea about upstream road conditions, and the construction of the infrastructure on the road can become expensive.

California Partners for Advanced Transit and Highways (PATH) has been investigating a look-down sensing scheme using discrete magnetic markers, with feed-forward preview control to reduce the feedback gains [7], [9], [10]. With preview, the lateral tracking problem is simplified into a regulation problem. The binary coding of the upcoming road geometry for the preview has also been suggested [9]. However, the binary coding of the road geometry using discrete magnetic markers makes the installation of the markers expensive, and the necessity of preview especially in highway driving conditions is still in question. In California, the recommended minimum radius for freeways is 900 meters, excluding ramps and intersections, and the equivalent maximum lateral acceleration of a vehicle on the curve at the speed of 100 km/h is only 0.086 g, even without super elevation. Therefore, considering the super elevation, the lateral acceleration of a vehicle at the curved section of a highway is very small. This paper studies the feasibility of minimizing the feed forward information and depending upon feedback control at least for the normal sections of the highway.

The discrete magnetic marking scheme has several advantages compared with the electrified wiring scheme. Since it is a passive system, it does not consume energy and the damage to any single magnet does not affect the overall system. The big disadvantage of the scheme is that the measurement is discontinuous from one marker to the next one, and the measurement error is also discontinuous.

This paper suggests a semicontinuous measurement method on discrete markers to minimize the effect of the big disadvantage. An observer is designed to smooth out the measurement error without introducing any phase lag. An adaptive look-down feedback control law is described which works well on a curved road without the feed-forward information about the road geometry. The robustness of the developed control law is verified empirically using a test vehicle for several vehicle speeds and environments.

II. Lateral Position Sensing

This section suggests a new lateral positioning scheme on the road reference system which consists of discrete magnetic markers embedded along the center of the test track at one-meter spacing.

Assuming that the markers are magnetic dipoles, the magnetic field around each marker can be described using polar coordinates (r, α) as (see Fig. 1) [15]:

$$H_r = k_m \frac{2 \sin \alpha}{r^3} \tag{1}$$

Manuscript received March 10, 1997; revised January 30, 1998.

The author is with TRW, Livonia, MI 48150-2172 USA (e-mail: ben.choi@trw.com).

Publisher Item Identifier S 0018-9545(00)11071-0.

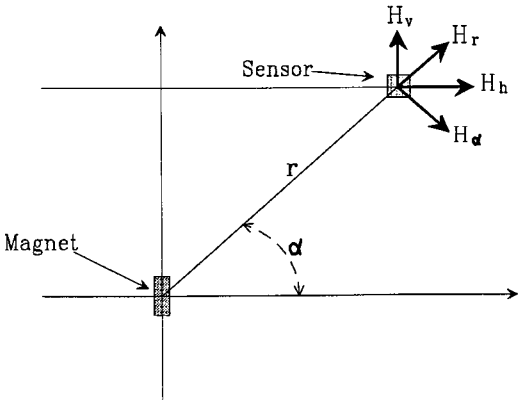

Fig. 1. Definition of coordinates.

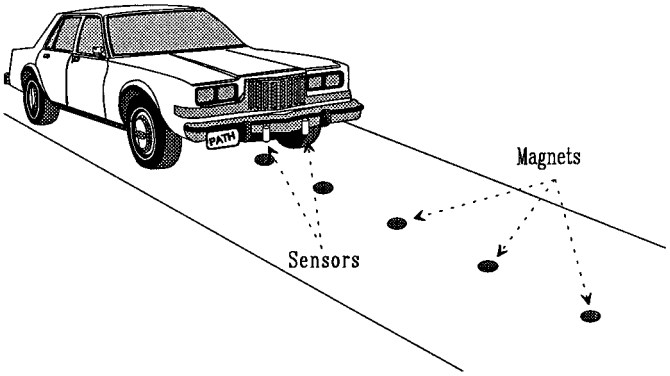

Fig. 2. Lateral positioning system.

$$H_\alpha = k_m \frac{\cos\alpha}{r^3} \tag{2}$$

where k_m is a constant proportional to the strength of the magnet. Therefore, the horizontal (H_h) and the vertical (H_v) component of the magnetic field can be written as:

$$H_h = k_m \frac{3\cos\alpha\sin\alpha}{r^3} \tag{3}$$

$$H_v = k_m \frac{2\sin^2\alpha - \cos^2\alpha}{r^3}. \tag{4}$$

As (3) and (4) show, each component of the field is a function of the strength (k_m), the distance to the sensor (r), and the angle (α). However, the ratio H_v/H_h is a function of just the angle (α)

$$\frac{H_v}{H_h} = \frac{2\sin^2\alpha - \cos^2\alpha}{3\cos\alpha\sin\alpha}. \tag{5}$$

Inspired by the fact that it is a function of just the angle, a robust and semi-continuous positioning scheme is suggested using two 3-axis magnetic sensors mounted under the front bumper of a vehicle (see Fig. 2).

Define the direction of the vehicle moving as x, and the lateral direction orthogonal to x as y, and the vertical direction as z. Similarly, define the components of the marker magnetic field measured at the sensor locations as (x_1, y_1, z_1) and (x_2, y_2, z_2) as Fig. 3 shows. Note that y_1 and y_2 are defined in an opposite

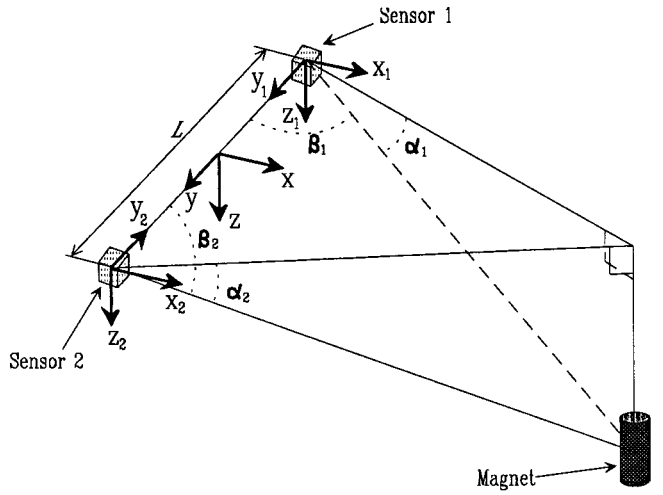

Fig. 3. 3-Dimensional sensing layout.

way. From (5), the angles from the sensors to the magnet (α_1 and α_2) with respect to the horizontal plane can be derived as:

$$\tan\alpha_i = \frac{3\eta_i + \sqrt{9\eta_i^2 + 8}}{4}, \qquad i = 1, 2 \tag{6}$$

where

$$\eta_i = \frac{|z_i|}{\sqrt{x_i^2 + y_i^2}}, \qquad i = 1, 2. \tag{7}$$

Define β_1 and β_2 on the triangle connecting the two sensors and the magnet (see Fig. 3). Geometrically, β_1 and β_2 are related to α_1 and α_2 as follows:

$$\cos\beta_i = \cos\alpha_i \frac{y_i}{\sqrt{x_i^2 + y_i^2}}, \qquad i = 1, 2. \tag{8}$$

Since β_1 and β_2 can be obtained, if the distance between the two sensors is defined as L, then the lateral position ($\triangleq d_y$) of the magnet with respect to the center of the two sensors can be derived as

$$d_y = \frac{L}{2} \frac{-\tan\beta_1 + \tan\beta_2}{\tan\beta_1 + \tan\beta_2}. \tag{9}$$

Since the magnetic field projected to the horizontal plane (x–y plane) makes concentric circles, the longitudinal position ($\triangleq d_x$) can also be obtained from a simple geometric relation as

$$d_x = L \frac{\dfrac{x_1}{x_2}\dfrac{x_2}{y_2}}{\dfrac{x_1}{y_1} + \dfrac{x_2}{y_2}} = L \frac{x_1 x_2}{x_1 y_2 + x_2 y_1}. \tag{10}$$

Therefore, the position of the vehicle with respect to the magnets can be measured continuously as long as the magnetic field is strong enough to be sensed. Moreover, the position measurement scheme derived in (9) and (10) is not affected by the variation of the strength of the magnets (k_m) and the vertical distance of the sensors from the magnets.

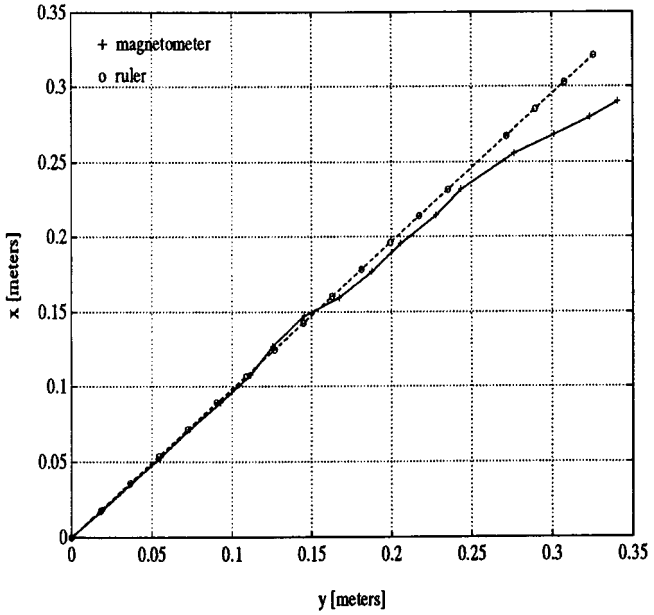

Fig. 4. Comparison of the magnetic sensing scheme with the direct measurement using a ruler.

The lateral measurement range can be extended by using only one of the two sensors, when the magnet is too far from the other sensor, using the nominal value of k_m. Consider the case that the magnet is too far from sensor 2, but not very far from sensor 1. With respect to the sensor 1, the angle α_1 can be calculated as in equation (6). Since the absolute value of the magnetic field ($\triangleq H_1$)

$$\begin{aligned} H_1 &\triangleq \sqrt{x_1^2+y_1^2+z_1^2} \\ &= \sqrt{H_{h_1}^2+H_{v_1}^2} \\ &= k_m \frac{\sqrt{4\sin^2\alpha_1+\cos^2\alpha_1}}{r_1^3} \end{aligned} \tag{11}$$

the distance from the sensor 1 to the magnet can be obtained as

$$r_1 = \left(\frac{k_m}{H_1}\right)^{1/3} (4\sin^2\alpha+\cos^2\alpha)^{1/6}. \tag{12}$$

Using r_1, the position (d_x, d_y) can be derived as

$$d_x = r_1\cos\alpha_1 \frac{x_1}{\sqrt{x_1^2+y_1^2}} \tag{13}$$

$$d_y = -\frac{L}{2} - r_1\cos\alpha_1 \frac{y_1}{\sqrt{x_1^2+y_1^2}}. \tag{14}$$

The accuracy of the positioning scheme given in equations (13) and (14) depends absolutely on the variation of k_m from its nominal value.

Fig. 4 shows the comparison of the semi-continuous magnetic sensing scheme described above with the direct measurement using a ruler on the x–y test bench. The magnetic sensors were mounted ± 0.15 meter apart from the center ($L = 0.3$ m) with 0.17 meter clearance to the top of the magnet. The test data shows that this measurement scheme derived in equations (9) and (10) (using two sensors, $|y| \leq 0.15$ m) is very accurate with the maximum error of only 2–3 mm. When using only one sensor ($|y| \geq 0.15$), the accuracy depends upon the deviation of K_m from the nominal value. However, the test results in Section VII shows that, during the closed-loop control, the lateral error is less than 0.1 meter, and within this range, the scheme developed in this section is very accurate.

The problem with the magnetic sensing is that the magnitude of the background earth magnetic field is not small compared to that of the marker magnetic field. Fig. 5 shows a typical pattern of the variation of the magnetic field when a vehicle, with the two magnetic sensors, is moving over one of the magnetic markers along the x axis with the marker centered between the sensors along the x axis. The variation of the magnitude and the direction of the earth magnetic field is very small around one location. Therefore, the horizontal component ($H_{h\_earth} = \sqrt{x_{earth}^2+y_{earth}^2}$) and the vertical component (z_{earth}) are almost constant. However, x_{earth} and y_{earth} are changing depending upon the direction in which the vehicle is heading. Assuming that the direction is not changing very fast, x_{earth} and y_{earth} can be obtained from the moving average of

$$\begin{aligned} (x_i', y_i') \triangleq \Big\{ &(x_{i\_meas}, y_{i\_meas}) \big| -\epsilon < \sqrt{x_{i\_meas}^2+y_{i\_meas}^2} \\ &- H_{h\_earth} < \epsilon, \qquad i=1,2 \Big\} \end{aligned} \tag{15}$$

for arbitrarily small positive ϵ. As Fig. 5 shows, the average of x_i'

$$\overline{x}_i' = x_{earth}, \qquad i=1,2. \tag{16}$$

However, the average of y_i

$$\overline{y}_1' = y_{earth} + \Delta \tag{17}$$

$$\overline{y}_2' = -y_{earth} + \Delta \tag{18}$$

where Δ is the residual magnetic field of the marker. Therefore, y_{earth} can be obtained from equations (17) and (18) as

$$y_{earth} = \tfrac{1}{2}(\overline{y}_1' - \overline{y}_2') \tag{19}$$

and the marker magnetic field (x_i, y_i, z_i) is defined as follows:

$$\begin{aligned} (x_i, y_i, z_i) = (&x_{i\_meas} - x_{earth}, y_{i\_meas} - y_{earth}, z_{i\_meas} \\ &- z_{earth}), \qquad i=1,2. \end{aligned} \tag{20}$$

The experimental results of this earth-field rejection scheme, tested on a curved test track, are shown in Figs. 6 and 7. In Fig. 6, x_{earth} and y_{earth} reflect the curve of the track shown in Fig. 9 exactly. Fig. 7 shows that the earth field is rejected exactly even when the marker magnetic fields are overlapping.

III. Vehicle Modeling

This section considers a classical linearized bicycle model with two degrees of freedom for the lateral dynamics of a vehicle. The curvature of the road is not considered in this study, since the effect of the curvature in the vehicle lateral control on the freeway is less than that of other modeling uncertainties and external disturbances.

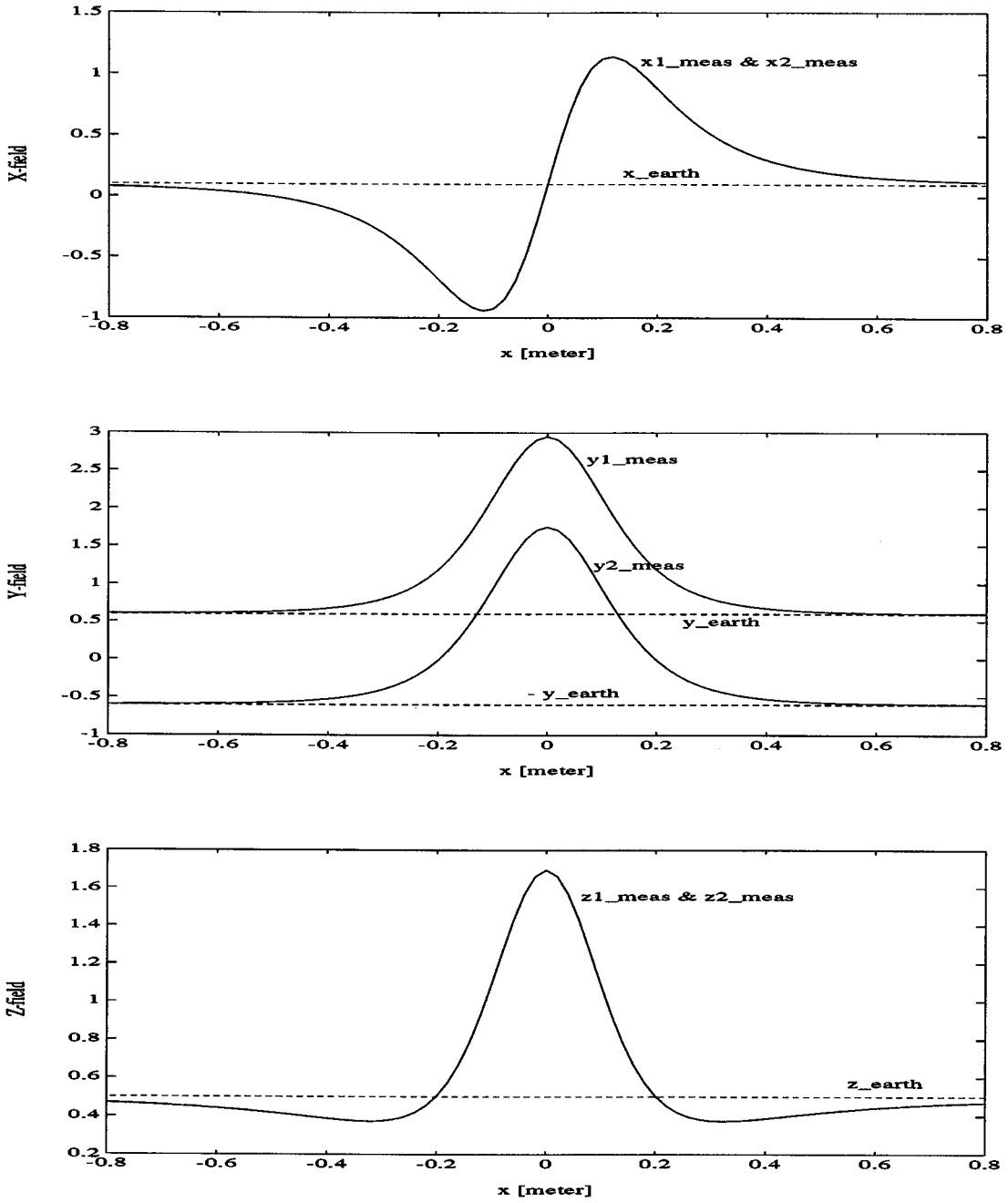

Fig. 5. Variation of magnetic field along the X-axis.

Defining the side-slip angle of a vehicle as q, the yaw rate as r, front wheel steering angle as δ_f, cornering stiffness of the front and the rear wheels as C_f and C_r, and the road adhesion factor as μ, and the vehicle velocity as v, then the lateral forces due to the slip (F_1, F_2) and to the yaw motion (F_3, F_4) can be derived as (see Fig. 8)

$$F_1 = C_f \mu (\delta_f - q) \tag{21}$$

$$F_2 = C_r \mu q \tag{22}$$

$$F_3 = C_f \mu \frac{l_f}{v} r \tag{23}$$

$$F_4 = C_r \mu \frac{l_r}{v} r. \tag{24}$$

If the normalized mass and the normalized angular moment of inertia of a vehicle are defined as $\tilde{m} \triangleq m/\mu$ and $\tilde{J} \triangleq J/\mu$, the governing equations of the vehicle dynamics can be written from F_1, F_2, F_3 and F_4 as follows:

$$\dot{r} = \frac{C_r l_r - C_f l_f}{\tilde{J}} q - \frac{C_r l_r^2 + C_f l_f^2}{\tilde{J} v} r + \frac{C_f l_f}{\tilde{J}} \delta_f \tag{25}$$

$$\dot{q} = -r - \frac{C_f + C_r}{\tilde{m} v} q + \frac{C_r l_r - C_f l_f}{\tilde{m} v^2} r + \frac{C_f}{\tilde{m} v} \delta_f. \tag{26}$$

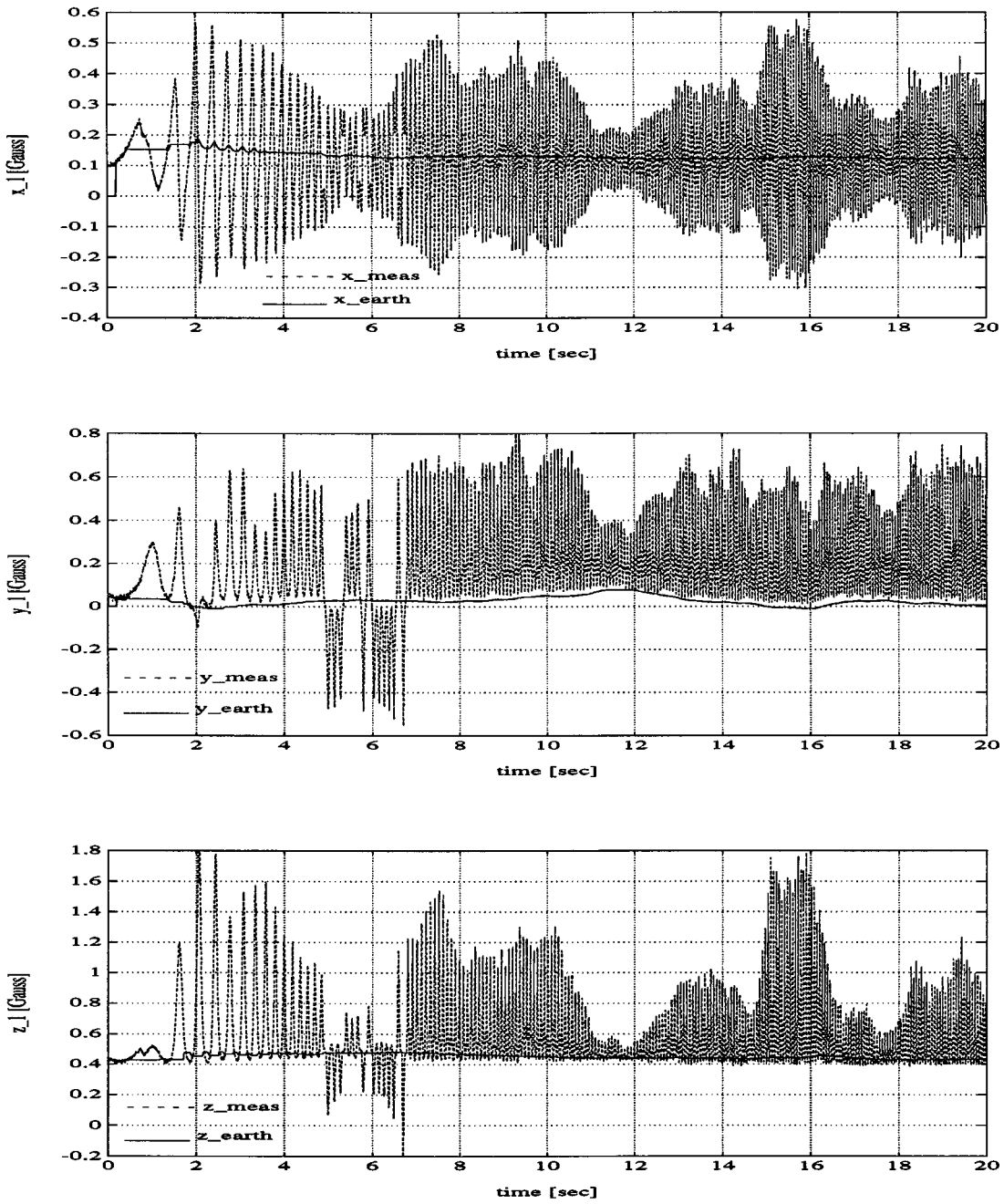

Fig. 6. The test result of earth magnetic field rejection (sensor 1).

IV. Lateral Control Law

Neglecting of the road curvature makes the control system very simple; the road curvature does not have to be coded into the magnetic markers. The system becomes even simpler by controlling the lateral error of the vehicle at the sensor location instead of the vehicle center of gravity; the yaw angle sensor can be eliminated from the control loop.

If the lateral tracking error of the vehicle at the sensor location is defined as d_s, the transfer function from the control input (δ_f) to the acceleration of the vehicle at the sensor location ($\ddot{d}_s$) can be derived from the relation:

$$\dot{d}_s = -v(q+\theta) - l_s r \tag{27}$$

where θ is the yaw angle ($\dot{\theta} \triangleq r$). Combining (25)–(27):

$$\ddot{d}_s(s) = -v\,\frac{q_0 s^2 + q_1 s + q_2}{s^2 + p_1 s + p_2}\,\delta_f(s) \tag{28}$$

where,

$$q_0 = \frac{C_f}{\tilde{m}v} + \frac{C_f l_f l_s}{\tilde{J}v} \tag{29}$$

$$q_1 = \frac{C_f C_r (l_r + l_s)(l_r + l_f)}{\tilde{m}\tilde{J}v^2} \tag{30}$$

$$q_2 = \frac{C_f C_r (l_r + l_f)}{\tilde{m}\tilde{J}v} \tag{31}$$

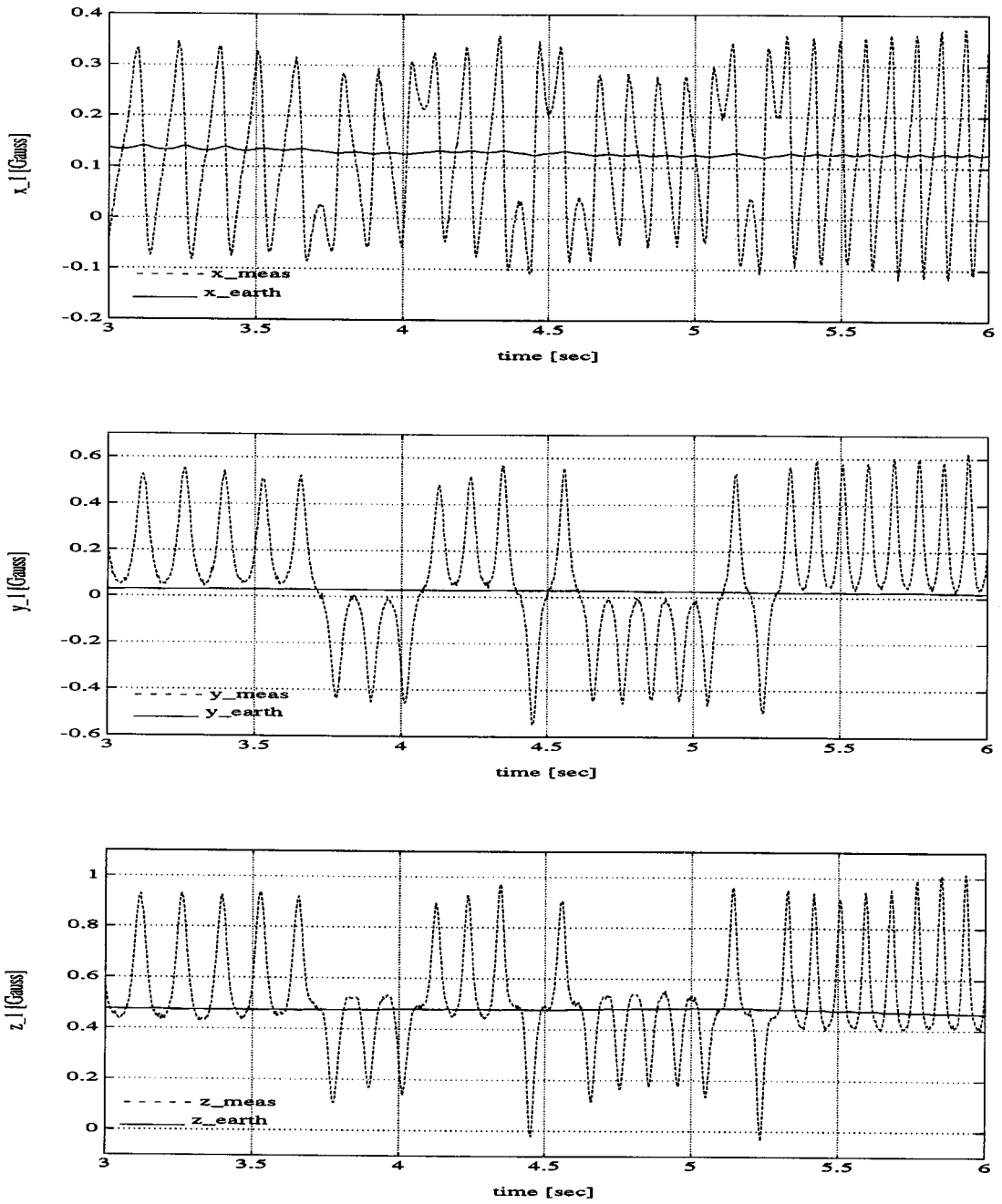

Fig. 7. The test result of earth magnetic field rejection (sensor 1, zoomed).

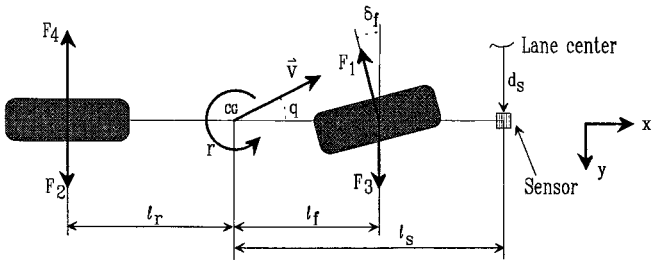

Fig. 8. Bicycle model of vehicle lateral dynamics.

$$p_1 = \frac{C_r + C_f}{\tilde{m}v} + \frac{C_r l_r^2 + C_f l_f^2}{\tilde{J}v} \tag{32}$$

$$p_2 = \frac{C_r l_r - C_f l_f}{\tilde{J}} + \frac{C_r C_f (l_r^2 + l_f^2) + 2C_r C_f l_r l_f}{\tilde{m}\tilde{J}v^2}. \tag{33}$$

Define the synthetic input δ_{syn} as:

$$\delta_{syn} \triangleq \frac{q_0 s^2 + q_1 s + q_2}{s^2 + p_1 s + p_2}\,\delta_f \tag{34}$$

then equation (28) can be simplified as

$$\ddot{d}_s = -v\delta_{syn}. \tag{35}$$

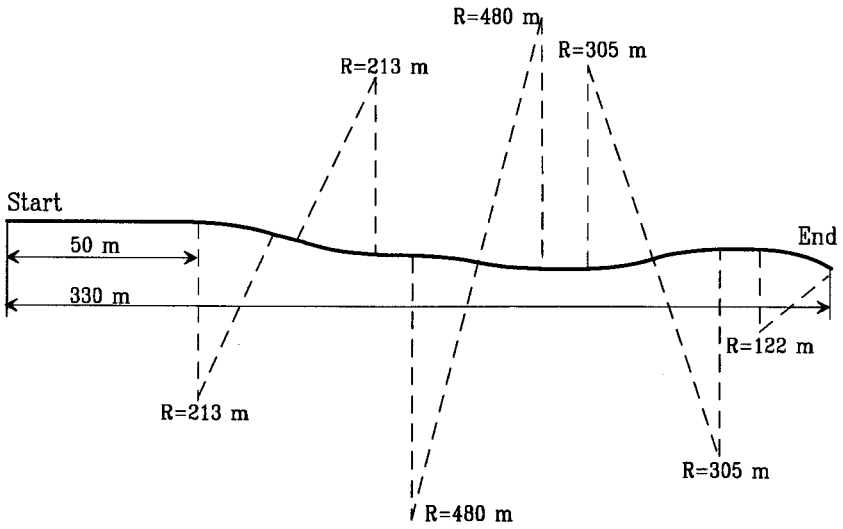

Fig. 9. The layout of RFS test track (not to scale).

Since it is a second order system, a PD type controller can be considered as follows:

$$\delta_{syn} \triangleq \frac{1}{v}(2\zeta\omega_n \dot{d}_s + \omega_n^2 d_s), \qquad \omega_n > 0,\ \zeta \geq 1 \tag{36}$$

From (35) and (36), the closed-loop transfer function becomes

$$\ddot{d}_s + 2\zeta\omega_n \dot{d}_s + \omega_n^2 d_s = 0 \tag{37}$$

and the error d_s converges to zero. Since the poles and the zeros of (34) are in the left half of a complex plane, the control law derived in (34) and (36) can be implemented.

V. Parameter Adaptation

Since the control law developed in Section IV is PD type, the closed-loop can have steady state tracking error due to the front wheel mis-alignments, unbalanced tire pressure, off-set error on the steering actuator or the steering angle sensor, side wind, super elevation of the road, road curvature, etc. Simply adding an integration term makes the closed-loop system slower or even unstable.

Since all the above-mentioned uncertainties are summarized as the unknown lateral force on the vehicle, the normalized vehicle model and the control law shown in (35) and (36) are modified as follows:

$$\ddot{d}_s = -v(\delta_{syn} + \delta_0) \tag{38}$$

$$\delta_{syn} \triangleq \frac{1}{v}(2\zeta\omega_n \dot{d}_s + \omega_n^2 d_s) - \hat{\delta}_0 \tag{39}$$

where δ_0 is an unknown parameter and $\hat{\delta}_0$ is the estimated value of δ_0. Due to the parametric uncertainty $\tilde{\delta}_0$ ($\triangleq \delta_0 - \hat{\delta}_0$), the closed-loop governing equation becomes

$$\ddot{d}_s = -2\zeta\omega_n \dot{d}_s - \omega_n^2 d_s - v\tilde{\delta}_0 \tag{40}$$

and the error d_s does not converge to zero.

In this section, an adaptation algorithm is developed to update $\hat{\delta}_0$ based upon a Lyapunov criterion. Define the positive-definite scalar function V

$$V \triangleq \frac{1}{2}(\dot{d}_s + \lambda d_s)^2 + \frac{1}{2k_a}\tilde{\delta}_0^2 \tag{41}$$

where λ is a constant that will be determined later. From (40) and (41)

$$\dot{V} = -(2\zeta\omega_n - \lambda)(\dot{d}_s + \lambda d_s)\left(\dot{d}_s + \frac{\omega_n^2 d_s}{2\zeta\omega_n - \lambda}\right) - \tilde{\delta}_0\left[v(\dot{d}_s + \lambda d_s) + \frac{1}{k_a}\dot{\hat{\delta}}_0\right]. \tag{42}$$

Choose λ such that

$$\lambda = \frac{\omega_n^2}{2\zeta\omega_n - \lambda} \tag{43}$$

i.e.,

$$\lambda = \left(\zeta \pm \sqrt{\zeta^2 - 1}\right)\omega_n \tag{44}$$

then, (42) becomes

$$\dot{V} = -\left(\zeta \mp \sqrt{\zeta^2 - 1}\right)\omega_n(\dot{d}_s + \lambda d_s)^2 - \tilde{\delta}_0\left[v(\dot{d}_s + \lambda d_s) + \frac{1}{k_a}\dot{\hat{\delta}}_0\right]. \tag{45}$$

If $\hat{\delta}_0$ is updated as follows:

$$\dot{\hat{\delta}}_0 = -k_a v(\dot{d}_s + \lambda d_s) \tag{46}$$

then,

$$\dot{V} = -\left(\zeta \mp \sqrt{\zeta^2 - 1}\right)\omega_n(\dot{d}_s + \lambda d_s)^2 \leq 0. \tag{47}$$

Therefore, the error d_s goes to zero, and if d_s goes to zero identically, $\hat{\delta}_0$ converges to δ_0 [see (40)].

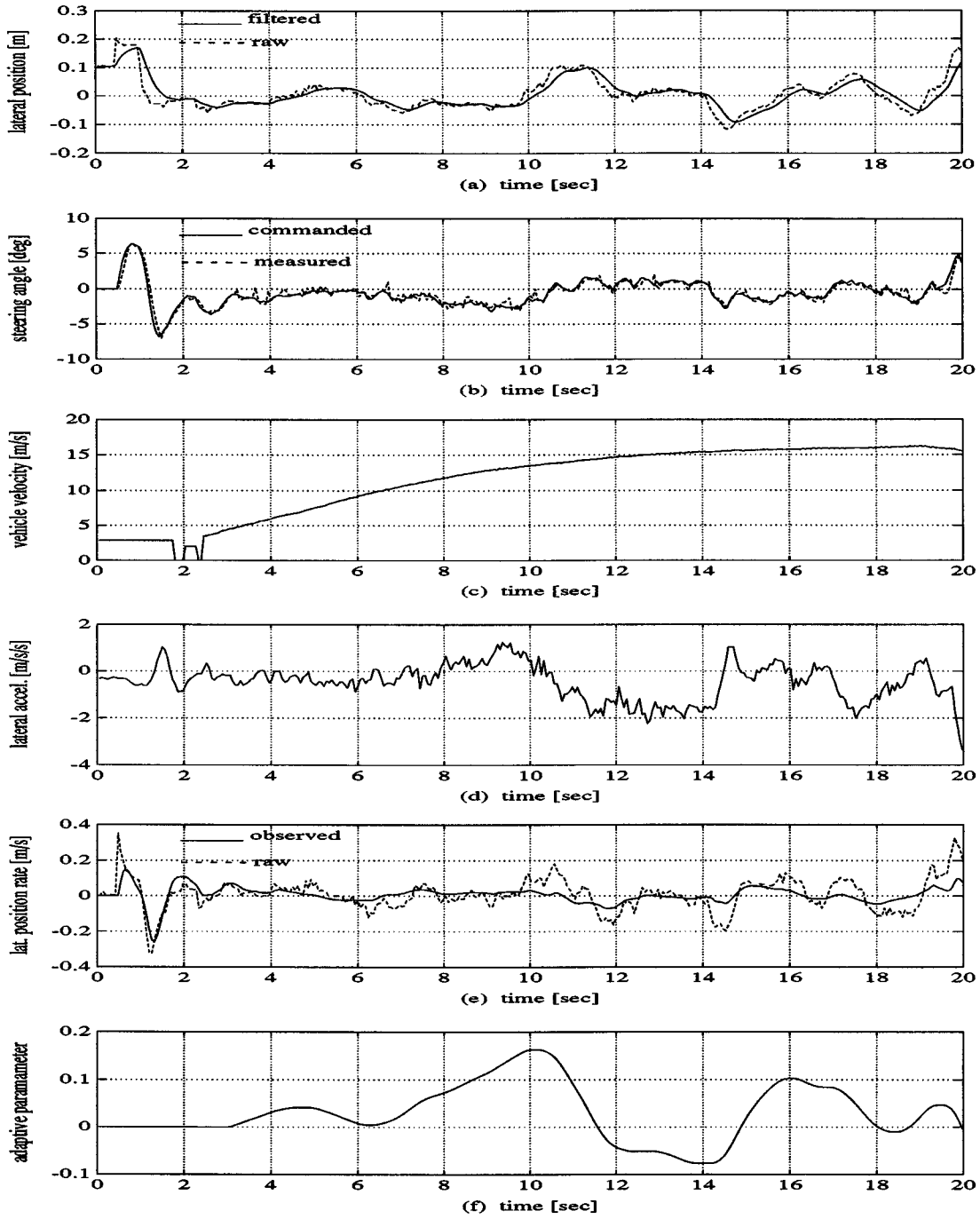

Fig. 10. Low speed closed-loop test at RFS.

VI. Control-Coupled Observer

The control law developed in Section IV needs d_s and $\dot{d}_s$, since it is PD type. The positioning error d_s can be obtained directly from the sensing scheme described in Section II. However, d_s is not smooth enough to be differentiated directly to get the D term ($\dot{d}_s$). Moreover, as mentioned in Section IV, the eigenvalues equivalent to (q_0, q_1, q_2) and (p_1, p_2) have negative real values, but they are lightly damped. Especially, the damping equivalent to (q_0, q_1, q_2) is decreasing in proportion to the vehicle velocity (v) and to the inverse of the cornering stiffness of the tires (C_f and C_r). Therefore, it is necessary to reject the low frequency measurement noise, as well as the high frequency noise, from $\dot{d}_s$ for the successful implementation of the control law derived in equation (36).

In this section, a control coupled-observer is described to filter out the low frequency noise on $\dot{d}_s$ without introducing the phase lag due to the filtering [3]. If the adaptive control law developed in Section V is working properly, the parameter $\hat{\delta}_0$ converges to δ_0. Therefore, the acceleration $\ddot{d}_s$ can be estimated

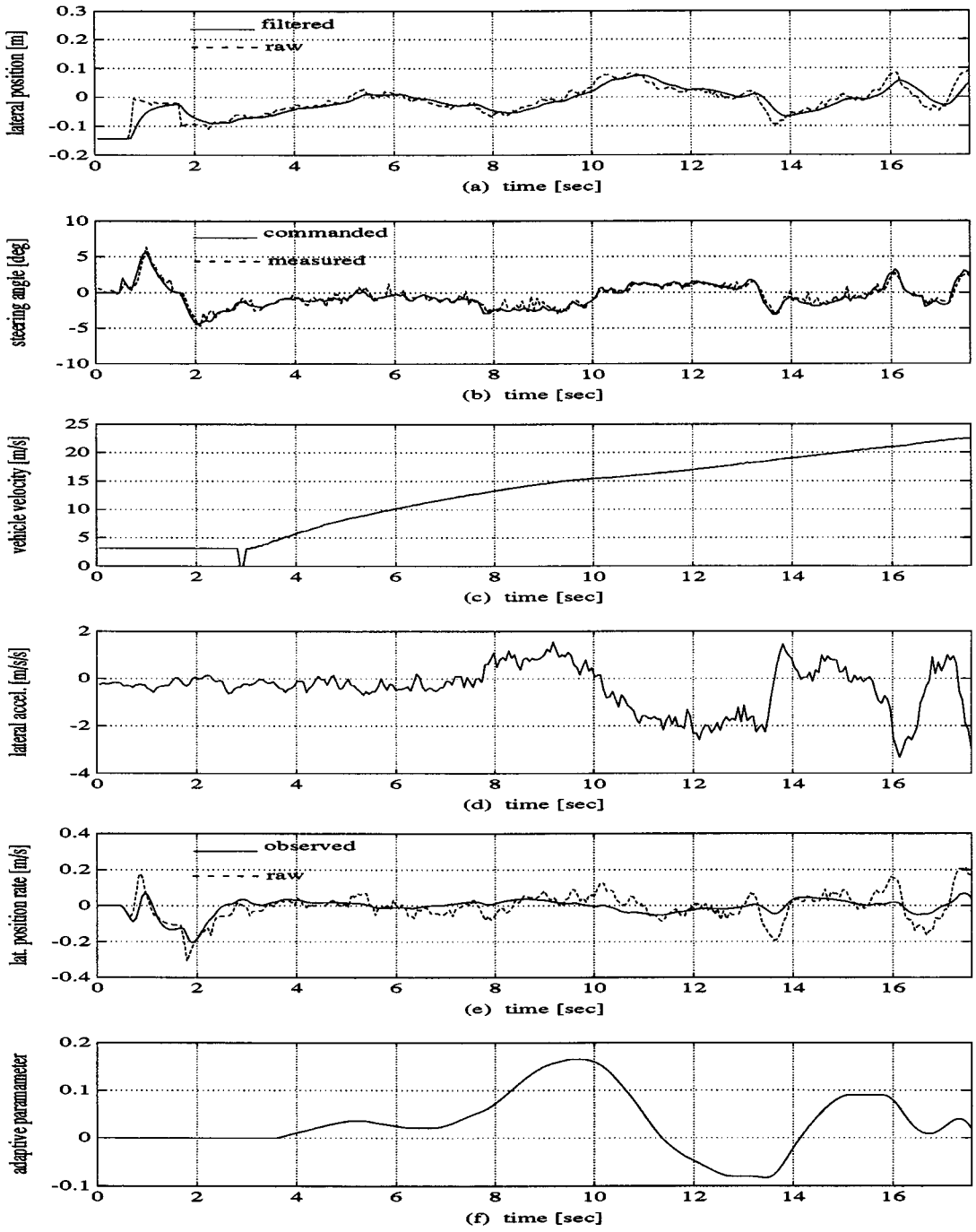

Fig. 11. High speed closed-loop test at RFS.

from (38) as

$$\dot{\hat{d}}_s = -v(\delta_{syn} + \hat{\delta}_0) \tag{48}$$

where $\dot{\hat{d}}_s$ means the estimation of $\ddot{d}_s$. Using $\dot{\hat{d}}_s$ as a feed-forward term, the observer of $\dot{d}_s$ is suggested as follows:

$$\dot{\hat{\dot{d}}}_s = -v(\delta_{syn} + \hat{\delta}_0) + k_s(\dot{d}_s - \dot{\hat{d}}_s), \qquad k_s > 0. \tag{49}$$

Considering the adaptation and the observation, the control law is finalized as follows:

$$\delta_{syn} = \frac{1}{v}(2\zeta\omega_n\dot{\hat{d}}_s + \omega_n^2 d_s) - \hat{\delta}_0. \tag{50}$$

Stability: Combining (38) and (49)

$$\ddot{d}_s - \dot{\hat{\dot{d}}}_s = -k_s(\dot{d}_s - \dot{\hat{d}}_s) - v\tilde{\delta}_0. \tag{51}$$

Therefore, the observer suggested in (49) is stable.□

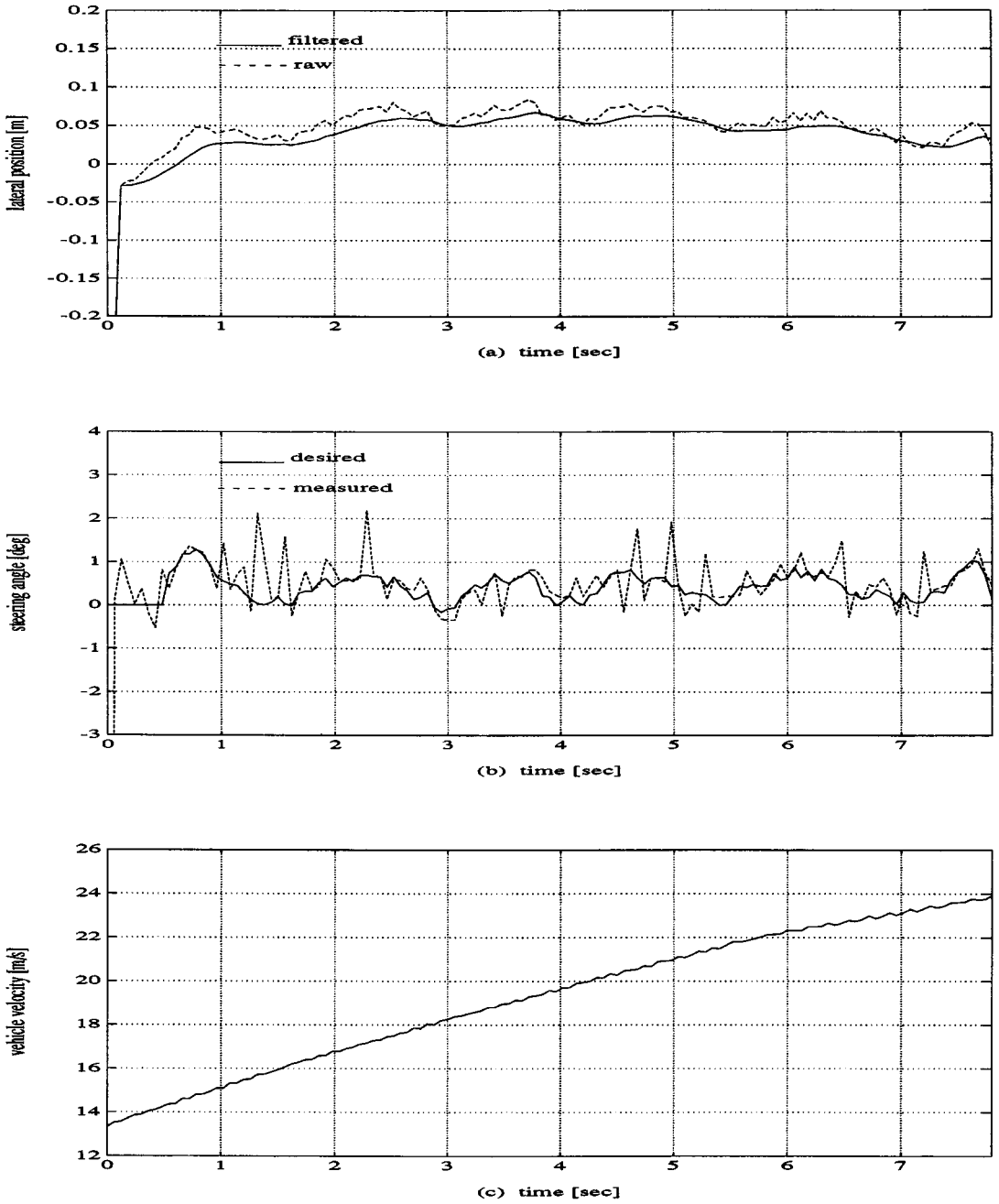

Fig. 12. High speed closed-loop test on a straight test track.

Convergence: Define a positive definite scalar function V as in equation (41), and λ as in equation (44), then:

$$\dot{V} = -\left(\zeta \mp \sqrt{\zeta^2 - 1}\right)\omega_n(\dot{d}_s + \lambda d_s)^2 - v(\dot{d}_s + \lambda d_s)\tilde{\delta}_0 + 2\zeta\omega_n(\dot{d}_s + \lambda d_s)(\dot{d}_s - \hat{\dot{d}}_s) - \frac{1}{k_a}\tilde{\delta}_0\dot{\tilde{\delta}}_0. \quad (52)$$

If $\tilde{\delta}_0$ is slowly varying, then $\dot{d}_s - \hat{\dot{d}}_s$ converges to $-(v/k_s)\tilde{\delta}_0$ [see (51)]. Therefore,

$$\dot{V} = -\left(\zeta \mp \sqrt{\zeta^2 - 1}\right)\omega_n(\dot{d}_s + \lambda d_s)^2 - \tilde{\delta}_0\left[v\frac{k_s + 2\zeta\omega_n}{k_s}(\dot{d}_s + \lambda d_s) + \frac{1}{k_a}\dot{\tilde{\delta}}_0\right]. \quad (53)$$

Define the adaptation law similar to (46) as

$$\dot{\tilde{\delta}}_0 \triangleq -k_a\frac{k_s + 2\zeta\omega_n}{k_s}v(\dot{d}_s + \lambda d_s) \triangleq -k_a' v(\dot{d}_s + \lambda d_s), \qquad k_a' > 0 \quad (54)$$

then,

$$\dot{V} = -\left(\zeta \mp \sqrt{\zeta^2 - 1}\right)\omega_n(\dot{d}_s + \lambda d_s)^2 \le 0. \quad (55)$$

Therefore, the error d_s converges to zero, $\hat{\dot{d}}_s$ to zero [see (49) and (50)], and finally $\hat{\tilde{\delta}}_0$ to δ_0 [see (51)].□

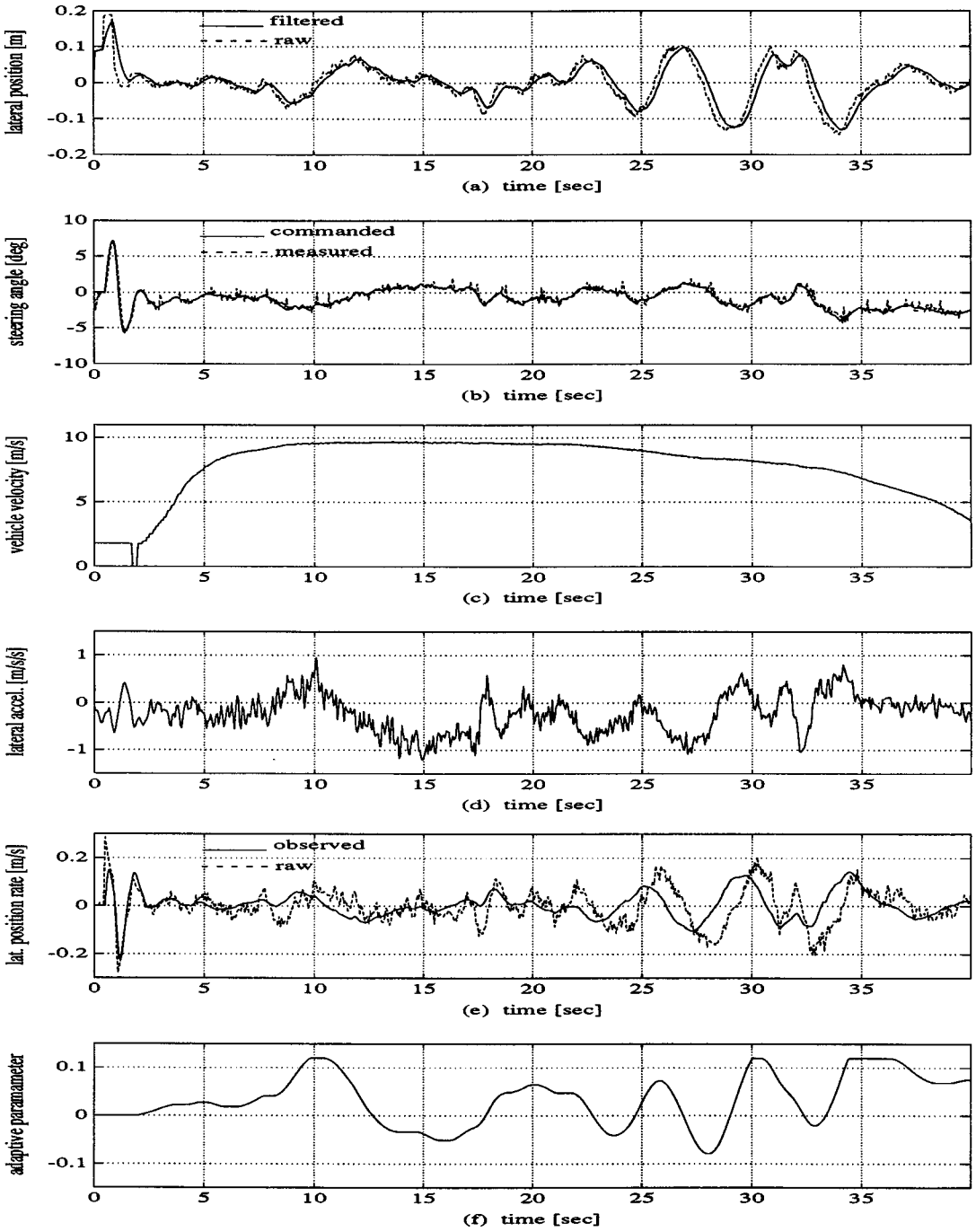

Fig. 13. Closed-loop test with a regular tire pressure (35 psi).

VII. Experimental Work

A. Test Setup

The vehicle lateral control tests were conducted using a 1989 Ford Crown Victoria, a typical rear-wheel-driven full-size sedan with very soft suspension. The vehicle was equipped with two magnetic sensors, 0.3 meters apart, under the front bumper as shown in Fig. 2. A lateral accelerometer was also installed to evaluate the acceleration during the maneuver with automatic control. However, the measured acceleration was not used for the control. The vehicle velocity was measured by tapping the wheel ABS sensor signal. The ABS sensor signal was very accurate above 4 m/s (9 mph).

The hydraulic loop of the conventional power steering system was modified to control the steering angle by the external servo valves. However, this steering actuation system was premature, and the performance was not very good; it had 30° phase lag at 2 Hz, and $\pm 1^\circ$ random errors in the command following.

The developed control law was implemented on a IBM-PC (166 MHz Pentium processor) with DOS and XIGNAL, a real-time kernel developed at the University of California, Berkeley (UCB). The interface to the sensors and the actuator

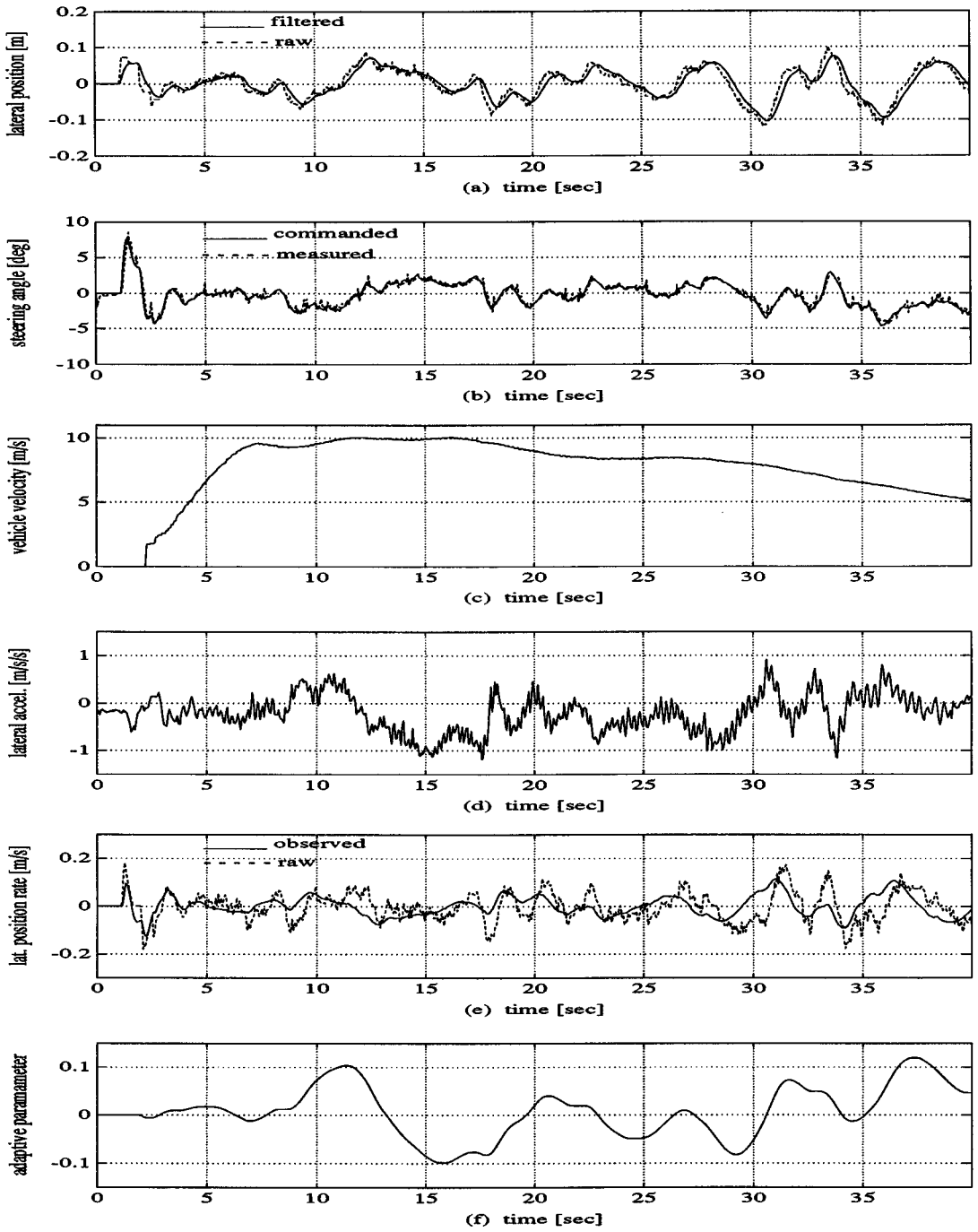

Fig. 14. Closed-loop test with a low tire pressure (15 psi).

was through National Instruments data acquisition boards. The data sampling and the control were running at 2 m/s loop-time. The control itself does not need 2 m/s loop time. However, 2 m/s loop time was chosen to pick up as many data as possible from each magnetic nail since measurement range of the magnetic field is only ± 0.3 meter in this case.

B. Vehicle Lateral Control

The lateral control tests were performed at the Richmond Field Station (RFS) test track of UCB and at another higher speed track near UCB. The profile of RFS track is as shown in Fig. 9. Much of the test track was designed based upon a previously existing dirt road at the site. The track is approximately 330 meter long and 5 meter wide. The permanent magnets with 2.2 cm diameter and 10.2 cm long were installed along the center of the track at 1 meter spacing.

Fig. 10 shows the result of the lateral control test on the RFS test track at a low speed using the adaptive control law and the observer developed in this study. Since the adaptive control law was designed assuming a linear system with a slowly varying parameter, while the real parameter can be varying

very quickly (e.g., road curvature), the adaptive parameter was bounded during the implementation. This control law has no feed-forward preview information, but as the result shows, the vehicle followed the center of the track very well with maximum 0.1 meter error [Fig. 10(a), filtered signal is used in the control] when the road curvature is changing stepwise very sharply from one direction to the opposite. The steering input remained very smooth [Fig. 10(b)], and the position-rate observer ($\hat{\dot{d}}_s$) was filtering out the measurement noise very well without a phase lag [Fig. 10(e)]. Fig. 10(f) shows the parameter adaptation. The adaptive routine was turned on at 3 s, adjusting the off-set error on the steering angle sensing (3–7 s), and estimating the road curvature (7–20 s).

Fig. 11 shows the result of the same testing, but at a higher speed up to 22 m/s (50 mph). Due to the higher speed, the lateral acceleration was increased. However, the lateral tracking error still remained at less than 0.1 meter, and the steering input command was also very smooth.

Fig. 12 shows the result of the same control law tested on the 150 meters straight stretch of another test track at an even higher speed up to 24 m/s (55 mph). Since the length of the track is very limited, the vehicle was accelerated to 13 m/s (30 mph) manually before the track, and then the automatic control was actuated at the starting point of the track. As Fig. 12(b) shows (data logging at 60 m/s loop-time), the steering actuator was not following the command very well. However, the closed-loop didn't become unstable, and the lateral positioning error was remaining at less than 0.05 meter.

As mentioned in Section VI, the high velocity and the low cornering stiffness make the damping of the control system very small, and the smaller damping makes the closed-loop system much less stable. The robustness of the control law to the variation of the cornering stiffness was also tested. Figs. 13 and 14 compare the behavior of the vehicle when the pressure of the tires was reduced from nominal 35 psi to 15 psi. In both cases, the control law was working very well, and the ± 0.1 meter errors for $t = 25$–40 sec were due to the very frequent stepwise change of the road curvature. In both figures, the observer ($\hat{\dot{d}}_s$) was filtering out the noise well, and even gave a little phase lead that was very helpful to make the closed-loop system more stable.

VIII. Conclusions

There are many advantages of vehicle lateral control with a preview information. However, it is very expensive or even impossible to have all the preview information, like road curvature, super elevation angle, and side wind which have major effects on the lateral control. Based upon the fact that, on the normal sections of the highway, the lateral force due to the super elevation angle or the side wind can be larger than that due to the road curvature, a look-down feedback adaptive controller was developed and tested on a passenger vehicle.

The test results show that it is feasible to eliminate the preview information on the normal sections of the highway. The suggested semicontinuous magnetic sensing scheme is simple but was working well on the high speed driving condition. Also, the developed control law is shown to be very robust to the change of the tire cornering stiffness, the critical and the most uncertain vehicle parameter in the lateral control.

References

[1] J. G. Bender, "An overview of systems studies of automated highway systems," *IEEE Trans. Veh. Technol.*, vol. 40, pp. 82–99, Jan. 1991.

[2] R. H. Byrne, C. T. Abdallah, and P. Dorato, "Experimental results in robust lateral control of highway vehicles," in *Proc. 34th Conf. Decision Control*, New Orleans, LA, 1995, pp. 3572–3575.

[3] S. B. Choi, "The design of a control coupled observer for the longitudinal control of autonomous vehicles," in *ASME Ann. Int. Congr. Exposition, Proc. Symp. Transportation Systems*, Atlanta, GA, 1996.

[4] E. D. Dickmans and A. Zapp, "Autonomous high speed road vehicle guidance by computer vision," in *Proc. IFAC 10th Ann. World Congr.*, Munich, Germany, 1987, pp. 221–226.

[5] R. E. Fentonk and R. J. Mayhan, "Automated highway studies at the Ohio University—An overview," *IEEE Trans. Veh. Technol.*, vol. 40, pp. 100–113, Jan. 1991.

[6] T. Hessburg, H. Peng, M. Tomizuka, W. Zhang, and E. Kamei, "An experimental studies on lateral control of a vehicle," in *Proc. Amer. Control Conf.*, Boston, 1991.

[7] A. Johnston *et al.*, "Automated vehicle guidance using discrete reference markers," *IEEE Trans. Veh. Technol.*, vol. VT - 28, Jan. 1979.

[8] R. J. Mayhan and R. A. Bishelk, "A two-frequency radar for vehicle automatic control," *IEEE Trans. Veh. Technol.*, vol. 31, Jan. 1982.

[9] H. Peng and M. Tomizuka, "Preview control for vehicle lateral guidance in highway automation," in *Proc. Amer. Control Conf.*, Boston, MA, 1991.

[10] ——, "Vehicle lateral control for highway automation," in *Proc. Amer. Control Conf.*, San Diego, CA, 1990, pp. 788–794.

[11] D. A. Pommerleau, "Progress in neural network-based vision for autonomous robot driving," in *Proc. Intelligent Vehicles Symp.*, Detroit, MI, 1992, pp. 391–496.

[12] D. H. Shin, S. Singh, and J. J. Lee, "Explicit path tracking by autonomous vehicles," *Robotica*, vol. 10, pp. 539–554, 1992.

[13] S. Shladover *et al.*, "Automatic vehicle control developments in the PATH program," *IEEE Trans. Veh. Technol.*, vol. 40, pp. 114–130, Jan. 1991.

[14] *Highway Design Manual*, 4th ed., California Department of Transportation.

[15] E. S. Shire, *Classical Electricity and Magnetism*. Cambridge, U.K.: Cambridge Univ. Press, 1960.

Seibum B. Choi received the B.S. degree in mechanical engineering from Seoul National University, Seoul, Korea, the M.S. degree in mechanical engineering from Korea Advanced Institute of Science and Technology, Seoul, Korea, and the Ph.D. degree in controls from the University of California, Berkeley in 1993.

From 1993 to 1997, he had worked for the development of Automated Vehicle Control Systems at the Institute of Transportation Studies at the University of California, Berkeley. Currently, he is with TRW, Livonia, MI, where he is working on the development of advanced vehicle braking control systems.